J Nanopart Res (2019) 21: 258
https://doi.org/10.1007/s11051-019-4699-7

RESEARCH PAPER

Particle size control of monodispersed spherical nanoparticles with MCM-48-type mesostructure via novel rapid synthesis procedure

Shewaye Yismaw · Richard Kohns · Denise Schneider · David Poppitz · Stefan G. Ebbinghaus · Roger Gläser · Ulrich Tallarek · Dirk Enke

Received: 10 July 2019 / Accepted: 29 October 2019 / Published online: 25 November 2019

Abstract Monodispersed spherical silica nanoparticles with a cubic mesostructure were synthesized in a fast and innovative way using triethanolamine (TEA) and the triblock copolymer Pluronic® F127 as particle growth inhibitors to control the particle size in a range from 420 to 62 nm. In this study, we described a synthesis of mesoporous silica nanoparticles (MSNs) with MCM-48 structure at room temperature with adequate control of particle monodispersity, shape, and size using TEA. Based on particle characterization, TEA can efficiently act as catalyst and at the same time as particle growth controlling additive. A mixture of TEA and Pluronic® F127 additives was used to obtain very small MSNs (62 nm), whereby the quality of MCM-48 silica is associated with the composition of the additives used and thus also with the final particle size. A finely dispersed and high-quality MCM-48 material with ~ 100% yield, excellent textural properties, and a particle size of 295 nm was synthesized within only 35 min using excess TEA as particle size controlling and dispersion agent together with ammonia as additional catalyst. Solvent extraction combined with ion exchange removed the surfactant efficiently. All prepared MSNs showed good textural properties, tunable particle sizes with narrow size distributions, and good dispersity in water, which make them highly promising as carriers for biomolecules in biomedical applications.

Keywords Mesoporous silica nanoparticles · MCM-48 structure · Particle size control · Surfactant removal · Triethanolamine · Biomedical relevance

S. Yismaw · R. Kohns · D. Schneider · D. Poppitz · R. Gläser · D. Enke (✉)
Institute of Chemical Technology, Universität Leipzig, Linnéstraße 3, 04103 Leipzig, Germany
e-mail: dirk.enke@uni-leipzig.de

S. Yismaw
Department of Chemistry, University of Gondar, P.O. Box 196, Gondar, Ethiopia

R. Kohns · U. Tallarek
Department of Chemistry, Philipps-Universität Marburg, Hans-Meerwein-Straße 4, 35032 Marburg, Germany

S. G. Ebbinghaus
Institute of Chemistry, Martin-Luther-Universität Halle-Wittenberg, Kurt-Mothes-Straße 2, 06120 Halle (Saale), Germany

Introduction

Mesoporous silica nanoparticles (MSNs) have fascinating properties such as high specific surface area, large pore volume, tunable particle size and pore diameter, flexible morphology, facile surface for functionalization, and good biocompatibility (Bharti et al. 2015; Ver Meer et al. 2010). Owing to these unique properties, they are widely applied in adsorption, catalysis, and biomedicine (Jin et al. 2017; Kuśtrowski et al. 2005; Verho et al. 2014; Wang et al. 2014; Zhang et al. 2017). The principal synthetic route for monodispersed silica particles was first discovered in 1968 by Stöber et al. (1968). Stöber's modified sol-gel method is the

most applicable synthesis approach for MSNs with various morphologies, particle sizes, and mesoporous structures. The preparation of sub-micrometer to sub-100-nm scaled monodispersed spherical MCM-41-type MSNs was studied extensively through modifying Stöber's synthesis (Das et al. 2014; Grün et al. 1997; Kobler et al. 2008; Lind et al. 2003; Qiao et al. 2009; Schiller et al. 2009; Uhlig et al. 2013). MCM-41-type MSNs were demonstrated to be good intracellular carriers for biomedical and pharmaceutical applications (Andersson et al. 2005; Angelos et al. 2008; Shahbazi et al. 2012; Yanes and Tamanoi 2012).

However, fewer investigations have been devoted to MCM-48-type MSN syntheses (with controlled particle diameter, morphology and mesophase structure) and their biomedical applications, as they are more difficult to synthesize. The synthesis of MSNs with defined cubic mesostructure and morphology requires precise control of the experimental conditions, including pH, temperature, stirring rate, stirring time, aging time, and concentrations of the templates (Boote et al. 2007; Hoffmann et al. 2006). Minor changes in these synthesis conditions may cause a significant difference in the properties of the final product. Recently, Luo et al. (2017) prepared high-quality MCM-48 materials by adjusting stirring rate, ethanol, and surfactant concentration. The presence of ethanol drives a mesophase transformation from hexagonal to mixed hexagonal/cubic, further to purely cubic, and finally to a mixed cubic/lamellar mesostructure. The simultaneous control of particle diameter, morphology, and mesophase structure by varying the amount of ethanol is still challenging. Kim et al. (2005) demonstrated the synthesis of a series of MCM-48-type MSNs, in which the environment-friendly and cheap nonionic co-surfactant poly(ethylene oxide)$_{106}$–poly(propylene oxide)$_{70}$–poly(ethylene oxide)$_{106}$ (Pluronic® F127) was used to efficiently control the particle size and particle dispersity in the surfactant cetyltrimethylammonium bromide (CTAB)–directed synthesis method. However, using a large amount of Pluronic® F127 in order to obtain small size particles impaired the morphology and led to the formation of polydispersed MSNs. Moreover, a synthesis of cubic mesostructured silica using the triblock copolymer Pluronic® P123 and *n*-butanol as structure-directing agents was reported (Kim et al. 2005; Kleitz et al. 2003). Guan et al. (2016, 2018) later used these two different copolymers (Pluronic® P123 and Pluronic® F127) as soft templates for the synthesis of large pore walnut-shaped macro-/mesoporous and bowl-like mesoporous poly-dopamine nanoparticles to create a composite with mesoporous carbon particles for a wide range of applications. Better control of monodispersity, morphology, and particle size in the synthesis of MSNs and the establishment of an appropriate surfactant removal method are imperative for biomedical applications.

Particularly mesoporous silica materials with three-dimensional (3D) porous networks (MCM-48, KIT-6) should have advantages over materials with one-dimensional arrays of pores (MCM-41, SBA-15) in various applications such as catalysis, adsorption, and biomedicine. The 3D pore system with cubic structure is more resistant to pore blocking and characterized by an improved mass transfer of the reactant molecules in the pore channels by providing more efficient (better connected) diffusion pathways. In addition, 3D pore structures offer more adsorption sites. Therefore, the 3D framework and the set of two interpenetrating pore systems make these materials promising for applications in biomedicine (Bandyopadhyay et al. 2005; Pajchel and Kolodziejski 2018; Uhlig et al. 2018; Vinu et al. 2008).

The current study focuses on the synthesis of monodispersed spherical MSNs with cubic mesostructure, excellent textural properties, and variable particle sizes using tetraethylorthosilicate (TEOS) as silica precursor, CTAB as template, NH_3 as alkaline catalyst, and TEA or/and Pluronic® F127 as particle growth inhibitors and dispersing agents respectively, at room temperature. We investigated the synthesis of particle size–controlled MCM-48-type MSNs using TEA as base catalyst, particle growth inhibitor, and dispersing agent for the first time. In addition to its alkaline catalytic activity like ammonia, it has been suggested that TEA is effective in controlling particle size and aggregation (instead of Pluronic® F127) while preserving the MCM-48-type mesostructure. Furthermore, a mixture of TEA and Pluronic® F127 may show synergistic effects in controlling the particle growth, which can lead to a reduction of the particle size of the monodispersed MSNs. The influence of TEA in combination with NH_3 as a base catalyst was also studied. Furthermore, the effects of experimental parameters like stirring rate and time, reaction time, and TEA concentration on the pore structure, textural properties, and particle size were investigated.

Experimental

Chemicals

Absolute ethanol (EtOH, 100%), hydrochloric acid (HCl, 37%) and ammonium hydroxide solution (NH_4OH, 25%) were purchased from VWR Chemicals (Darmstadt, Germany). Tetraethylorthosilicate (99%) was received from abcr (Karlsruhe, Germany). Pluronic® F127 ($EO_{106}PO_{70}EO_{106}$, BioReagent) and cetyltrimethylammonium bromide (99%) came from Sigma-Aldrich (Steinheim, Germany). Triethanolamine (99%) was provided by Acros organics (Geel, Belgium). Deionized water was used for all experiments. All chemicals were used without further purification.

Synthesis of monodispersed spherical MSNs

Initially, a control sample with high-quality MCM-48 structure was prepared via a surfactant assembled sol-gel process in a modified Stöber solution containing CTAB, TEOS, NH_3, water, and ethanol without any additive. Briefly, 0.5 g CTAB was dissolved in water (96 mL) and absolute ethanol (43.3 mL). After complete dissolution, aqueous ammonia solution (11.2 mL, 25 wt.%) was added. TEOS (2 mL) was added quickly under vigorous stirring (1000 rpm), which was continued for 1 min after TEOS addition. The molar ratio of the final reaction mixture was 1 TEOS:0.15 CTAB:32.7 NH_3:598.3 H_2O:27.8 C_2H_5OH. The reaction mixture was kept at room temperature (25 °C) under static conditions for 24 h. Afterwards, the white product was separated by centrifugation and washed repeatedly with water and ethanol within a couple of minutes to prevent further particle growth and remove unreacted residues.

To obtain finely dispersed MSNs with adjustable particle size, TEA or/and Pluronic® F127 were added to similar reaction mixtures (control sample), keeping the composition and all other conditions constant. Herein, four different reaction compositions were used:

1) Adding Pluronic® F127 (2 g) for comparison of its effect with TEA.
2) Replacing NH_3 by TEA (16 mL) (volume ratio TEOS/TEA = 1/8). TEA acts as base catalyst and particle growth controller taking over the role of both NH_3 and Pluronic® F127.
3) Using a mixture of Pluronic® F127 (2 g) and TEA (16 mL).
4) TEA (16 mL) was used to control the particle growth and particle aggregation in the presence of NH_3 with respect to the control sample (only NH_3).

Finally, the pore-generating agent CTAB was removed by reflux solvent extraction in an ethanol solution (100 mL) containing aqueous HCl (6 mL, 37%) or NH_4NO_3 (1.5 g) under stirring at 60 °C for 3 h. The purpose of using NH_4NO_3 or HCl in ethanol is to break the electrostatic forces between the oligomeric silicate anions and the cationic head groups (CTA^+) of CTAB (Lang and Tuel 2004). To ensure complete surfactant removal, the extraction step was repeated twice and the particles were washed three times with ethanol after each extraction step. For selected samples, a Soxhlet extraction approach using acidic ethanol solution (for 24 h) was applied for comparison. All samples were finally dried under vacuum at 80 °C.

Characterization

A Leo Gemini 1530 scanning electron microscope (SEM) (Zeiss, Oberkochen, Germany) was used to analyze the morphology, monodispersity, aggregation, and particle size of the synthesized MSNs. The particle size of all samples was determined from the SEM images using ImageJ software by a random measurement of 80 to 100 particles. Transmission electron microscopy (TEM) analysis was performed on JEM2100Plus (JEOL, Tokyo, Japan) instrument operated at a 200-kV acceleration voltage. The particles were dispersed in ethanol and supported on a lacey-carbon TEM grid. Silica nanosphere suspensions in water were measured using the Colloidal Dynamics AcoustoSizer II (AZR II) (Colloidal Dynamics, Ponte Vedra Beach, FL) to obtain hydrated particle sizes and their distributions. The device determines the particle size and zeta potential from electroacoustic and ultrasonic attenuation measurements. To assure the removal of the surfactant molecules, thermogravimetric analysis (TGA) was carried out for selected samples in a STA 409 thermobalance (Netzsch, Selb, Germany) with a heating rate of 10 °C per minute under air. For further confirmation, selected samples were analyzed before and after CTAB removal using elemental analysis (Vario EL III, Elementar Analysensysteme, Langenselbold, Germany) and attenuated total reflectance Fourier transform infrared spectroscopy (ATR-FTIR) with a Vector 22 spectrometer (Bruker, Billerica, MA). Low-angle powder X-ray

diffraction (XRD) measurements were performed at room temperature on a D8 Advance diffractometer (Bruker AXS, Karlsruhe, Germany) operating with Cu-K_α radiation in the range $2\theta = 0.4–10.0°$ with a step size of 0.01° and a counting time of 1 s/step (LynxEye-Detector). Nitrogen (N_2) physisorption measurements were performed using a Quantachrome Autosorb iQ (Quantachrome, Boynton Beach, FL). Prior to the sorption, measurements all samples were treated under vacuum at standard conditions of 250 °C for 10 h. The specific surface areas were calculated using the Brunauer-Emmett-Teller (BET) method in the range of $p/p_0 = 0.05–0.35$ and the total pore volume was obtained at the maximum relative pressure $p/p_0 = 0.98$. The non-local density functional theory (NLDFT) method was applied to estimate the pore diameters using the adsorption branch model considering N_2 sorption at − 196 °C in silica with cylindrical pore geometry.

Results and discussion

The synthesis of MSNs with tunable porosity and particle size as well as good dispersity (particularly < 200 nm) was highlighted in previous studies, since materials are interesting for biomedical applications including cell imaging, disease diagnosis, and drug/gene/protein storage or delivery (Du and He 2011; He and Shi 2011; Polshettiwar et al. 2010; Qiao et al. 2009; Xu et al. 2013). Therefore, the development of innovative and improved synthesis methods for the manufacture of such MSNs constitutes a major challenge in order to meet the ever-increasing requirements. One of the focal points represents the effectiveness of the synthesis procedure in terms of duration and costs. Among other things, the use of other or additional chemicals can change and improve these factors. Also, most of the previous works rely on calcination as a surfactant removal method after the synthesis of MCM-48-type MSNs (Kim et al. 2010; Luo et al. 2017; Peng et al. 2012). Recently, the development of organic-inorganic hybrid nanomaterials with multiple functionalities has attracted more attention, e.g., in biomedical applications or catalysis (Borodina et al. 2015; Kickelbick 2007). Calcination for template removal is not practicable for such materials as the required organic functionalization is lost during the heat treatment. Hence, a mild surfactant removal method should be established to make the entire process more efficient.

Influence of TEA and Pluronic® F127

The use of growth inhibitor additives and functional organosilanes (Kim et al. 2005; Möller et al. 2007; Urata et al. 2009; Zhang et al. 2011; Effati and Pourabbas 2012) improves the particle dispersity and helps to control the particle size of MSNs. Therefore, the complexing agents TEA and Pluronic® F127 were used as additives to achieve a fine dispersion and to efficiently control the particle size. Table 1 shows the properties of the reference material (MSN-NH_3) and samples prepared using both additives under the same reaction conditions.

The reference MSN-NH_3 (a) exhibits highly aggregated, large spherical particles (Fig. 1) with an average particle diameter about 420 nm. In contrast, finely dispersed and relatively small-sized MSNs were formed using Pluronic® F127 or/and TEA as particle growth and aggregation controlling additives. The average particle diameter of the spheres was significantly reduced from 420 to 143 nm by using Pluronic® F127 (MSN-F127 (b)). Alternatively, a replacement of NH_3 by TEA (MSN-TEA (c)) leads to the formation of monodispersed highly spherical particles with a decrease of the particle diameter to 186 nm. This indicates that TEA efficiently controls the material's spherical nature, particle diameter, monodispersity, and aggregation. Apparently, it acts as a weak base that catalyzes the hydrolysis and condensation rates of the molecular silica precursors. Moreover, it is a silica oligomer surface capping or chelating ligand that controls aggregation and further growth of silica particles and thus influences the growth mechanism of the MSNs (Möller et al. 2007). The steric effect of the catalyst molecules also plays an important role in controlling the final particle size of the silica. Since TEA is sterically more demanding and less nucleophilic, it results in the formation of smaller particles, while the use of the sterically less demanding NH_3, which has a stronger alkaline character than TEA, leads to the formation of larger MSNs (Nandy et al. 2014).

The sample MSN-FT (d) (Table 1) was synthesized by adding both Pluronic® F127 and TEA to the reaction mixture, which resulted in a small particle diameter of 62 nm. This indicates that the use of a mixture of these additives allows better particle size control with a narrow distribution while maintaining textural properties.

Based on SEM images and AZR II measurements (Fig. 1), as well as N_2 sorption results (Fig. 2b, c), TEA

Table 1 Porosimetry data and physical properties of MSNs

Sample	S_{BET} (m^2 g^{-1})[a]	V_{meso} (cm^3 g^{-1})[a]	d_{meso} (nm)[a]	x_p (nm)[b]	x_p (nm)[c]
MSN-NH_3 (a)	1245	0.86	3.4	420	535 (±29)
MSN-F127 (b)	1264	0.89	3.2	143	293 (±9)
MSN-TEA (c)	1252	0.76	3.2	186	297 (±8)
MSN-FT (d)	1388	0.81	3.4	62	167 (±3)

[a] BET surface area (S_{BET}), mesopore size (d_{meso}), and volume (V_{meso}) based on nitrogen physisorption measurements

[b] Average particle size (x_p) estimated from SEM images

[c] Average particle size (x_p) determined by AZR II with corresponding standard deviation

can efficiently play the role of both the catalyst NH_3 and the organic additive Pluronic® F127. Furthermore, TEA has improved the particle monodispersity and shape. The low-angle XRD patterns of the samples with different particle diameters indicate an ordered mesostructure, whereby the reference (a) exhibits an XRD pattern with well-resolved peaks (in the 2θ range of 2–6°) of a highly ordered 3D MCM-48 cubic mesopore structure with the space group $Ia\bar{3}d$; the peaks correspond to the lattice planes (211), (220), (420), and (332) (Fig. 2a) (Boote et al. 2007; Kim et al. 2005; Kim et al. 2010; Solovyov et al. 2005).

For MSNs prepared using F127 (b) or TEA (c) and a mixture of both (d), the XRD diffraction peaks appear broadened and with decreased intensity, but can still be referred to as MCM-48-like mesostructures. The broadening of the diffraction peaks can be attributed to the limited long-range order of the pores imposed by the relatively small size of the particles that leads to a decrease in the reflection domains of the mesophase. It might also correlate with the disordering of the material that reflects the formation of a low-quality cubic mesostructure (Kim et al. 2010; Lelong et al. 2008; Qiao et al. 2009). Furthermore, the slight shift of the peaks towards smaller angles in the case of MSN-TEA and MSN-FT reflects a structural deviation of the pores compared with the ordered materials of type M41S. A study by Möller et al. (2007), in which a reduction in particle diameter caused the peak shift to the lower 2θ values, showed an analogical effect.

All samples reveal type IV nitrogen sorption isotherms according to the IUPAC nomenclature with a sharp capillary condensation step ($p/p_0 = 0.18$–0.38) and uniform mesopore diameters between 3.2 and 3.4 nm (Fig. 2b, c). This characterizes high-quality periodic mesoporous materials with a narrow pore size distribution (Brunauer et al. 1940). A sharp secondary capillary condensation step above a relative pressure of $p/p_0 = 0.9$ is observed for samples prepared using particle size controlling agents, where the hysteresis loop

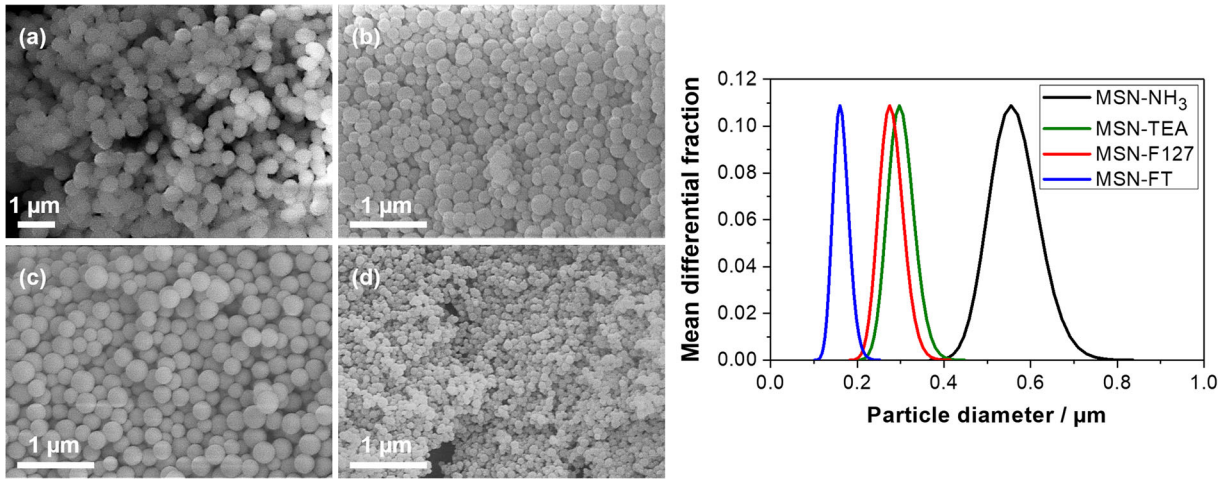

Fig. 1 SEM images of the reference material (**a**) and the particle growth–controlled samples prepared with TEA (**b**), Pluronic® F127 (**c**) and a mixture of both (**d**), and the corresponding AZR II–based particle size distributions

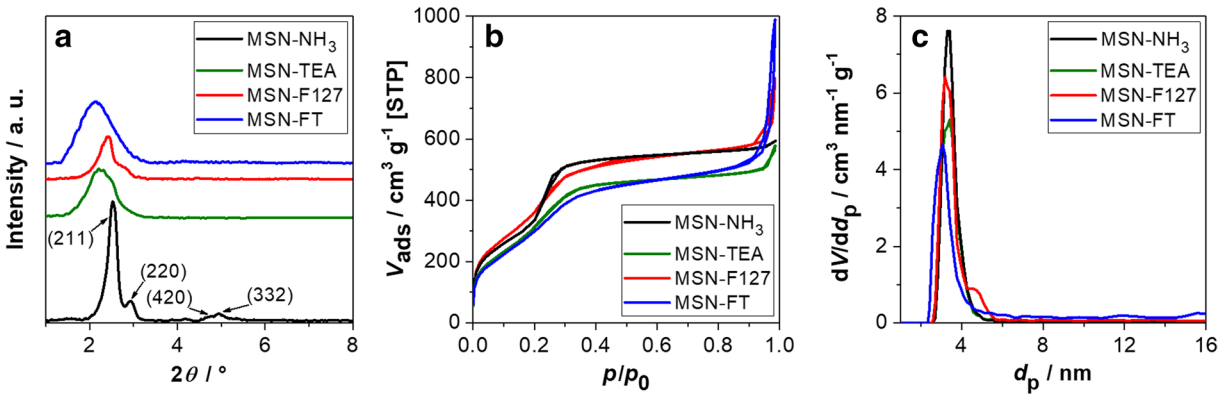

Fig. 2 Structural analysis by XRD patterns (**a**), N_2 physisorption isotherms (**b**), and the corresponding NLDFT pore size distributions (**c**) for the MSNs with decreasing particle size

becomes broader and higher with decreasing particle diameter. This is related to the interparticle voids observed with decreasing particle size (Luo et al. 2017; Qiao et al. 2009), a result consistent with the SEM and AZR II–based measurements.

However, the sample prepared using TEA (MSN-TEA) showed a less pronounced capillary condensation step at lower p/p_0 than MSN-NH_3 and MSN-F127. This indicates that the interaction of TEA with silica prevents particle aggregation and polydispersity and inhibits particle growth, but reduces the order of the final mesopore structure (observed at lower p/p_0).

One of the major challenges associated with the synthesis of MSNs in this work was the low yield of the final products in a single batch. This might be related to the use of a diluted solution, incomplete hydrolysis, and condensation in the presence of growth controlling additives as well as loss of material during surfactant removal and sampling. The final yield of samples synthesized at room temperature was only about 54%, particularly when additives were used to control the particle growth and aggregation. This severe problem was effectively solved using TEA as particle size controller and dispersion agent together with NH_3 as the catalyst that predominantly controlled the hydrolysis and condensation reactions of silicate species, whereby the yield of this synthesis could be enhanced to almost 100%. This reaction route also facilitated the better investigation of the efficiency of TEA as a particle growth controlling agent in the presence of NH_3. Using this composition, a stable milky suspension was observed within 2 min after TEOS addition. Therefore, one sample was prepared for a reaction time of 24 h (NH_3-TEA-24 h (e)) and the other for 35 min (NH_3-TEA-35 min (f)), keeping all other reaction conditions constant. It is shown that a significant change in the reaction time has barely any effect on the textural properties and product yields (Table 2). This indicates that a stable material with well-defined mesopore structure can be formed already within a very short reaction period at higher pH values (pH ~ 12.8). As illustrated in the SEM pictures (Fig. 3), monodispersed and non-aggregated nanoparticles with an average particle diameter of ~ 295 nm were obtained within 35 min. The extended reaction time of 24 h did not influence the particle size (~ 303 nm) or the porosimetry properties. Thus, it appears that the excess amount of TEA can efficiently control the particle growth through chelating the silica precursor and improve the particle dispersion by interaction with the silica surface without affecting

Table 2 Textural properties of the MSN samples to investigate the influence of the reaction time

Sample	S_{BET} (m^2 g^{-1})[a]	V_{meso} (cm^3 g^{-1})[a]	d_{meso} (nm)[a]	x_p (nm)[b]
MSN-NH_3 (a)	1245	0.86	3.4	420
NH_3-TEA-24 h (e)	1245	0.86	3.4	303
NH_3-TEA-35 min (f)	1360	0.88	3.4	295

[a] BET surface area (S_{BET}), mesopore size (d_{meso}), and volume (V_{meso}) based on nitrogen physisorption measurements

[b] Average particle size (x_p) estimated from SEM images

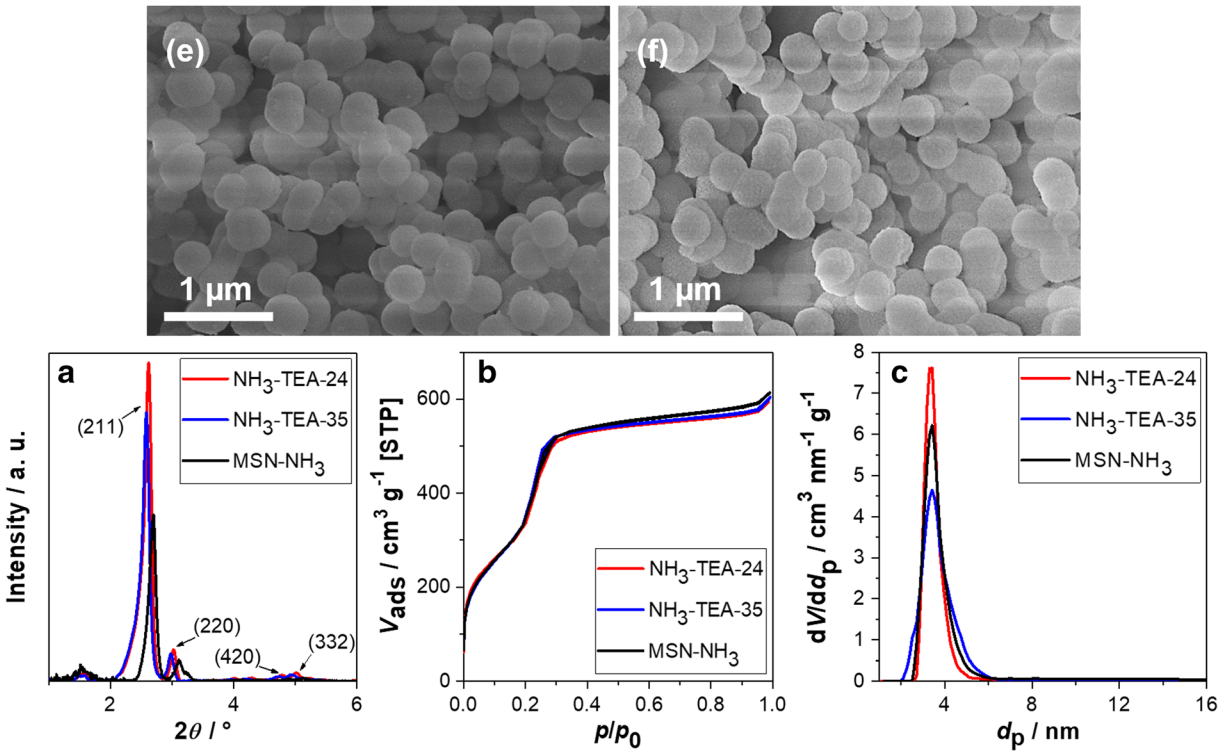

Fig. 3 SEM images of the samples prepared with TEA during a synthesis time of 24 h (**e**) and 35 min (**f**) with the corresponding XRD patterns (**a**), N_2 physisorption isotherms (**b**), and NLDFT pore size distributions (**c**)

the quality of the mesopore structure (Möller et al. 2007; Pardo-Tarifa et al. 2017).

However, some interconnected particles were formed especially for a long reaction time (e) in addition to the uniform spherical particles. This might be associated with the high content of anionic species due to the high pH in the solution, which causes the high cleavage rate of siloxane bonds (Si-O-Si) or the dissolution of particles (Schubert 2015). The initially formed, spherical primary particles aggregate and form larger secondary particles after reaching a certain size instead of further growth. This phenomenon was not significant for sample (f). Due to the formation of such interconnected particles, the AZR II analysis was not applicable.

The XRD results revealed the formation of highly ordered cubic $Ia\bar{3}d$ structures of MCM-48 silica nanoparticles (Fig. 3a), which was achieved in a short period of time (35 min) using NH_3 and TEA in the synthesis solution. Nitrogen sorption isotherms of samples (e) and (f) showed typical type IV isotherms characterized by pronounced capillary condensation steps at relative pressures between 0.18 and 0.38 (Fig. 3b). Based on these results, we conclude that this synthesis route can be used as best alternative time-saving method for finely dispersed high-quality MCM-48 materials with good textural properties, enhanced yield, and controlled particle diameter. In particular, the reduced synthesis time due to the dual-templating synthesis should be emphasized, which would also make a technical realization much more practical and attractive.

TEM observations for selected samples, MSN-NH_3 (a), MSN-FT (d), and NH_3-TEA-35 (f), revealed well-defined spherical particles with an average particle size of 409, 56, and 306 nm, respectively (Fig. 4). Furthermore, lattice plane imaging was realized for (a) and (f) with relatively large particle sizes but not for the small size nanoparticles (d). The lattice plane imaging for MSN-FT was not feasible possibly due to lack of the order structures because the small particle size limits the long-range ordering of the pores (Qiao et al. 2009). A higher degree of ordering has been observed for the larger particles. This result confirms the impact of the particle size on the periodicity of the pore structure. However, the results of the TEM analysis are comparable with the information provided by SEM, AZR II, and XRD.

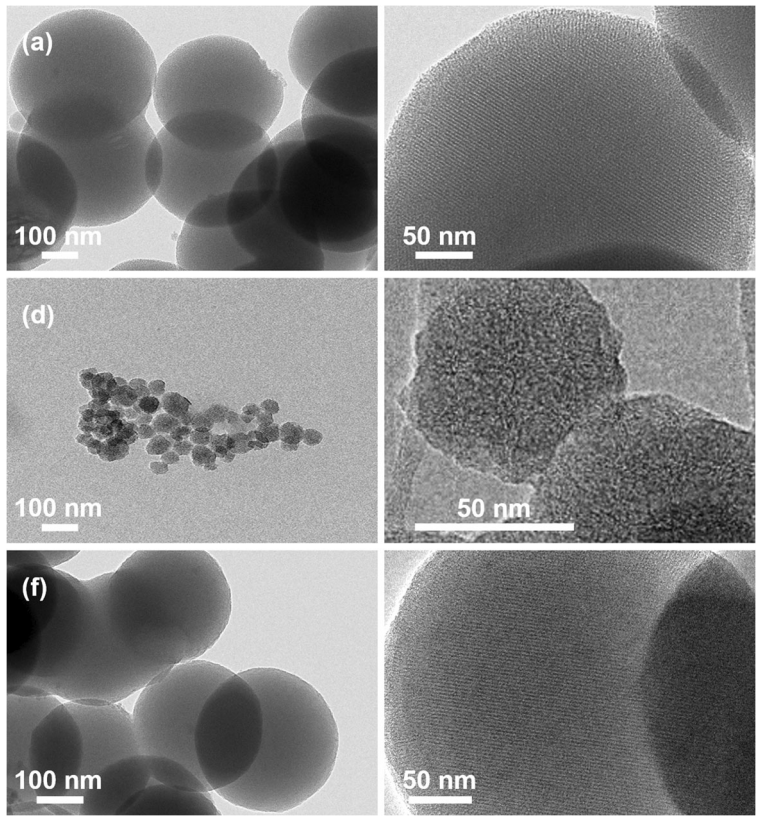

Fig. 4 TEM images for the reference sample (**a**) and samples prepared by adding a mixture of TEA and Pluronic® F127 (**d**) and only TEA but with a reaction time of 35 min (**f**). The figures with the scale bar of 50 nm (right) show the particle pore structure

In general, the particle size of cubic like mesoporous silica nanoparticles can be controlled by growth controlling additives in conjunction with the adjustment of reaction parameters. In this work, a comprehensive material characterization was performed using various techniques to demonstrate this. Previous works also showed different approaches implemented to control the particle growth during synthesis as summarized in Table 3.

Surfactant removal

In view of a subsequent modification process, an attempt was made to establish a low temperature solvent extraction method. A Soxhlet extraction method using an acidic (HCl) ethanol solution for 24 h (referred to as (sox)) and a reflux method using an acidic or ammonium nitrate containing ethanol solution at 60 °C for 3 h (referred to as (ref)) were tested. For the sample

Table 3 Summary of some particle size controlling synthesis methods with tunable particle size ranges estimated from SEM images

Methods	Particle size range (nm)	References
Particle growth inhibitors (Pluronic® F127 and/or TEA)	62–420	This study
Optimization of co-solvent and surfactant molar ratio	223–353	Luo et al. (2017)
Application of functional organosilanes	50–700	Cho et al. (2011); Effati et al. (2012)
Adjustment of physical parameters in a binary surfactant system	70–500	Kim et al. (2010)
Variation of the catalyst	25–245	Qiao et al. (2009); Nandy et al. (2014)
Variation of the silicate/surfactant concentration	65–740	Nooney et al. (2002)
Adjustment of reaction time, temperature, silica source-catalyst ratio	45–150	Möller et al. (2007)
Variation of catalyst concentration and co-solvent content	30–500	Guan et al. (2012)

prepared with Pluronic® F127, both textural properties (pore size, specific surface area, and pore volume) and mesopore structure were strongly affected by the reflux extraction method (MSN-F127(ref)) compared with the Soxhlet method (MSN-F127(sox)). This can be clearly observed from the XRD patterns (Fig. 5a), where a collapse of the MCM-48 framework is evidencedand the N_2 sorption isotherms and the corresponding pore size distributions supported this observation (Fig. 5b, c). As confirmed by the N_2 sorption t-plot analysis, micropores were formed in the reflux extraction method instead of the unique mesopores, which causes a shift of the pore size distributions to smaller values. In contrast, none of the samples prepared using TEA showed any defects in the textural properties and mesopore structure after application of the reflux method, as seen in the XRD patterns (Figs. 2a and 3a), so that TEA also has a positive effect in this respect. Nevertheless, the XRD pattern, the N_2 sorption isotherm, and the pore size distribution of the sample after Soxhlet extraction (MSN-F127(sox)) in acidic ethanol was comparable with the control sample MSN-NH_3(sox) (Fig. 5).

To verify the removal of CTAB after these extraction methods, FTIR measurements, thermogravimetric, and elemental analyses were performed. According to the TGA (Fig. 6a), the sample exhibited a weight loss of about 39% before CTAB extraction, with the majority occurring before reaching 400 °C. The initial weight loss at low temperatures, up to 200 °C, was due to the removal of physically adsorbed solvent and residual precursors. A pronounced weight loss was observed between 200 and 300 °C, which can be associated with the removal of the organic fractions of the decomposing CTAB at ~ 243 °C. The weight loss in the temperature range of 300–600 °C is due to the decomposition of residual organic molecules and the further condensation of adjacent silanol groups (Möller et al. 2007). After CTAB extraction (MSN-NH_3), the sample revealed a weight loss of only ~ 5% up to 600 °C, possibly due to the removal of remaining solvent molecules, showing that the surfactant was almost completely removed by the extraction process.

In addition, FTIR measurements were applied to confirm the complete removal of CTAB and to further evaluate the efficiency of the surfactant removal methods, as seen in the FTIR absorption spectra (Fig. 6b) of the non-extracted sample (MSN-CTAB) and the samples after CTAB removal (MSN-sox and MSN-ref). The strong bands at 1100 and 804 cm^{-1} are associated with the stretching vibrations of Si-O-Si in the silica framework and the band at 970 cm^{-1} is attributed to Si-OH bending vibrations (Doadrio et al. 2006). The two strong bands of MSN-CTAB at 2915 and 2848 cm^{-1} are due to the asymmetric and symmetric vibrations of CH_2 units from the CTAB molecules, while the band at 1470 cm^{-1} is due to the CH_2 bending vibrations of the surfactant. These absorption peaks of the non-extracted sample at 2915, 2848, and 1470 cm^{-1} can be used to prove the successful removal of the surfactant. It can be seen that the intensity of these CH_2-stretching and bending vibration bands has almost completely disappeared after both Soxhlet (MSN-sox) and reflux (MSN-ref) extraction indicating a complete CTAB removal. The minor absorbance of CH vibrations observed at 2999 cm^{-1} after surfactant removal might be due to other organic residues.

To corroborate the successful removal of the surfactant, the weight percentages of nitrogen, carbon, and

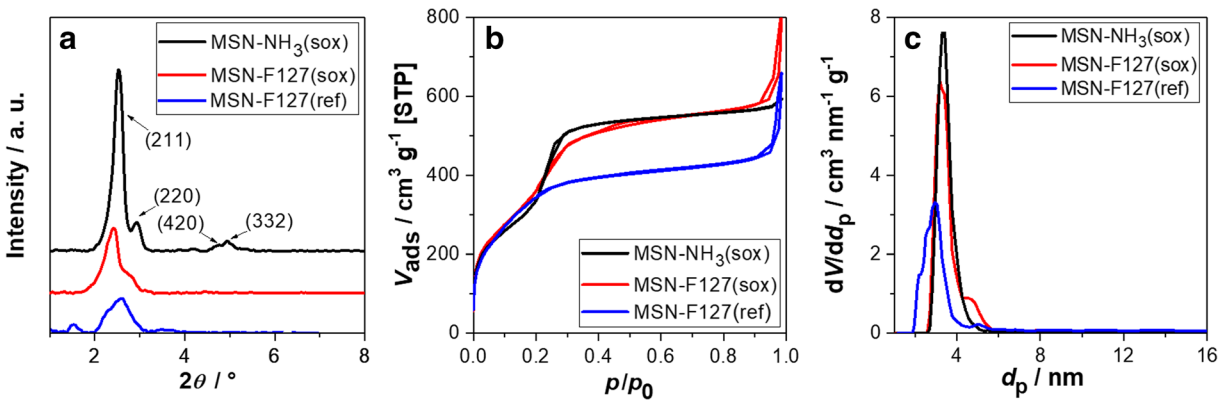

Fig. 5 XRD patterns (**a**), N_2 physisorption isotherms (**b**), and the respective NLDFT pore size distributions (**c**) for comparison of the reflux and Soxhlet surfactant extraction methods with the reference material

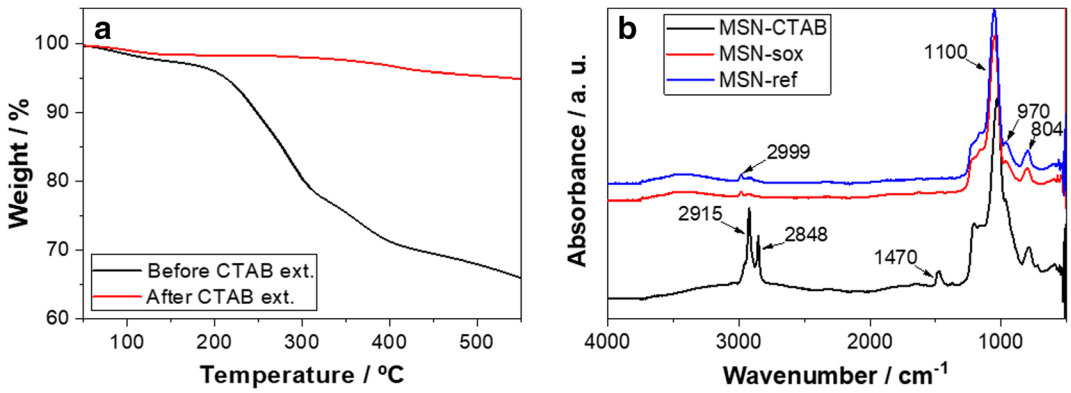

Fig. 6 Thermogravimetric analysis (**a**) for a selected sample before and after reflux surfactant extraction and FTIR spectra (**b**) for comparison of the reflux and Soxhlet surfactant extraction methods with a non-extracted material

hydrogen were determined by elemental analysis before and after both extraction methods (Table 4). The nitrogen content should be assigned to the quaternary ammonium head group of CTAB so that the data suggest that the surfactant was removed with both extraction variants. The complete loss of nitrogen after the reflux method (MSN-ref) using an ammonium nitrate/ethanol solution leads to the conclusion that this procedure is the most suitable for this surfactant removal. The presence of 0.2 wt.% nitrogen and an increase in the content of carbon by 2.1 wt.% as well as of hydrogen by 0.7 wt.% (with respect to the reflux extraction method) after Soxhlet extraction can be due to traces of residual surfactant, which were not clearly detected in the FTIR spectra. The traces of remaining surfactant might be due to the lower ion exchange rate between H^+ and CTA^+ compared with the exchange between NH_4^+ and CTA^+, which reduces the extraction efficiency for CTAB in the Soxhlet method. The percentage of carbon/hydrogen, CH stretching, and bending vibrations in the FTIR spectrum at 2999 cm^{-1} after surfactant removal might originated in residual organic reaction components such as non-hydrolyzed ethoxy groups. The FTIR results are in line with thermogravimetric and elemental analyses as well as N_2 sorption analysis revealing high pore volume (0.7–0.9 $cm^3\ g^{-1}$) and BET surface area (> 1100 $m^2\ g^{-1}$) after CTAB removal.

Table 4 Results of the elemental analysis before the removal of the surfactant and after both extraction procedures

Sample	N-%	C-%	H-%
MSN-CTAB	1.8	32.1	6.6
MSN-ref	0.0	5.8	1.7
MSN-sox	0.2	7.9	2.4

However, as soon as even a small amount of organic residues remains in such materials, especially of those as toxic as CTAB, the MSNs are not suitable for biomedical applications. Complete removal could finally be achieved by the usual calcination or treatment with hydrogen peroxide. Nevertheless, in our case, we will show in future work that the surfactant could fulfill even a beneficial function if it remains in the pore space during surface functionalization. This would allow a subsequent external surface modification of the MSNs. After this functionalization, the surfactant can be selectively removed from the inner surface via the extraction route shown here, resulting in a material containing the organic functionality exclusively on the external surface of the nanoparticles.

Conclusions

In this study, the particle size of mesoporous silica nanoparticles was adjusted and controlled through the addition of growth inhibitors and by adapting the reaction conditions. This allowed us to generate stable spherical particles with MCM-48 mesostructures. The use of TEA as particle growth controlling additive or/and base catalyst as well as substitute for the usually employed Pluronic® F127, and NH_3, respectively, was successful in the synthesis of MCM-48-like MSNs. The utilization of a mixture of Pluronic® F127 and TEA resulted in small-sized MSNs with a particle diameter of 62 nm from SEM analysis. Finely dispersed MSNs with MCM-48-type cubic mesopore structure, controlled

particle diameter, and excellent textural properties were synthesized in only 35 min, which resulted in significant time-savings and established a rapid method for the synthesis of high-quality MSNs. In addition, in contrast to the commonly used organic removal procedures, a solvent extraction method was successfully applied for an efficient surfactant removal while retaining key textural properties of the MSNs.

Overall, the synthesized MSNs show good textural properties, adjustable particle sizes between 420 and 62 nm, excellent dispersity in water, and colloidal stability and can act as potential carriers for biomolecules. These characteristics enable functionalization of the MSNs with stimuli responsive polymers, with the aim to use these composite materials for controlled and targeted drug delivery studies.

Acknowledgements The authors would like to thank Christian Splith from the University of Leipzig for the contribution in taking SEM images of the nanoparticles.

Funding information The authors received financial support from the Institute of Chemical Technology, Faculty of Chemistry and Mineralogy, University of Leipzig, and the German Academic Exchange Service (DAAD) for this research work.

Compliance with ethical standards

Conflict of interest The authors declare that they have no conflict of interest.

References

Andersson J, Areva S, Spliethoff B, Lindén M (2005) Sol-gel synthesis of a multifunctional, hierarchically porous silica/apatite composite. Biomaterials 26:6827–6835. https://doi.org/10.1016/j.biomaterials.2005.05.002

Angelos S, Liong M, Choi E, Zink JI (2008) Mesoporous silicate materials as substrates for molecular machines and drug delivery. Chem Eng J 137:4–13. https://doi.org/10.1016/j.cej.2007.07.074

Bandyopadhyay M, Birkner A, van den Berg MWE, Klementiev KV, Schmidt W, Grünert W, Gies H (2005) Synthesis and characterization of mesoporous MCM-48 containing TiO_2 nanoparticles. Chem Mater 17:3820–3829. https://doi.org/10.1021/cm0484854

Bharti C, Nagaich U, Pal AK, Gulati N (2015) Mesoporous silica nanoparticles in target drug delivery system: a review. Int J Pharm Investig 5:124–133. https://doi.org/10.4103/2230-973X.160844

Boote B, Subramanian H, Koodali RT (2007) Rapid and facile synthesis of siliceous MCM-48 mesoporous materials. Chem Commun:4543–4545. https://doi.org/10.1039/B706633C

Borodina E, Karpov SI, Selemenev VF, Schwieger W, Maracke S, Fröba M, Rößner F (2015) Surface and texture properties of mesoporous silica materials modified by silicon-organic compounds containing Quarternary amino groups for their application in base-catalyzed reactions. Microporous Mesoporous Mater 203:224–231. https://doi.org/10.1016/j.micromeso.2014.10.009

Brunauer S, Deming LS, Deming WE, Teller E (1940) On a theory of the van der Waals adsorption of gases. J Am Chem Soc 62:1723–1732. https://doi.org/10.1021/ja01864a025

Cho E-B, Volkov DO, Sokolov I (2011) Ultrabright fluorescent silica mesoporous silica nanoparticles: control of particle size and dye loading. Adv Funct Mater 21:3129–3135. https://doi.org/10.1002/adfm.201100311

Das D, Yang Y, O'Brien JS, Breznan D, Nimesh S, Bernatchez S, Hill M, Sayari A, Vincent R, Kumarathasan P (2014) Synthesis and physicochemical characterization of mesoporous SiO_2 nanoparticles. J Nanomater 2014:1–12. https://doi.org/10.1155/2014/176015

Doadrio JC, Sousa EMB, Izquierdo-Barba I, Doadrio AL, Perez-Pariente J, Vallet-Regí M (2006) Functionalization of mesoporous materials with long alkyl chains as a strategy for controlling drug delivery pattern. J Mater Chem 16:462–466. https://doi.org/10.1039/B510101H

Du X, He J (2011) Spherical silica micro/nanomaterials with hierarchical structures: synthesis and applications. Nanoscale 3:3984–4002. https://doi.org/10.1039/C1NR10660K

Effati E, Pourabbas B (2012) One-pot synthesis of sub-50 nm vinyl- and acrylate-modified silica nanoparticles. Powder Technol 219:276–283. https://doi.org/10.1016/j.powtec.2011.12.062

Grün M, Lauer I, Unger KK (1997) The synthesis of micrometer- and submicrometer-size spheres of ordered mesoporous oxide MCM-41. Adv Mater 9:254–257. https://doi.org/10.1002/adma.19970090317

Guan B, Cui Y, Ren Z, Qiao Z, Wang L, Liu Y, Huo Q (2012) Highly ordered periodic mesoporous organosilica nanoparticles with controllable pore structures. Nanoscale 4:6588–6596. https://doi.org/10.1039/C2NR31662E

Guan B, Yu L, Lou XWD (2016) Formation of asymmetric bowl-like mesoporous particles via emulsion-induced Interface anisotropic assembly. J Am Chem Soc 138:11306–11311. https://doi.org/10.1021/jacs.6b06558

Guan B, Zhang SL, Lou XWD (2018) Realization of walnut-shaped particles with macro−/mesoporous open channels through pore architecture manipulation and their use in electrocatalytic oxygen reduction. Angew Chem Int Ed 57:6176–6180. https://doi.org/10.1002/anie.201801876

He Q, Shi J (2011) Mesoporous silica nanoparticle based nano drug delivery systems: synthesis, controlled drug release and delivery, pharmacokinetics and biocompatibility. J Mater Chem 21:5845–5855. https://doi.org/10.1039/C0JM03851B

Hoffmann F, Cornelius M, Morell J, Fröba M (2006) Silica-based mesoporous organic-inorganic hybrid materials. Angew Chem Int Ed 45:3216–3251. https://doi.org/10.1002/anie.200503075

Jin X, Wang Q, Sun J, Panezai H, Bai S, Wu X (2017) Dual (pH- and temperature-) stimuli responsive nanocarrier with bimodal mesoporous silica nanoparticles core and copolymer shell for controlled ibuprofen-releasing: fractal feature and diffusion mechanism. Microporous Mesoporous Mater 254:77–85. https://doi.org/10.1016/j.micromeso.2017.05.003

Kickelbick G (2007) Hybrid materials: synthesis, characterization and applications. Wiley-VCH, Weinheim

Kim T-W, Kleitz F, Paul B, Ryoo R (2005) MCM-48-like large mesoporous silicas with tailored pore structure: facile synthesis domain in a ternary triblock copolymer-butanol-water system. J Am Chem Soc 127:7601–7610. https://doi.org/10.1021/ja042601m

Kim T-W, Chung P-W, Lin VS-Y (2010) Facile synthesis of monodisperse spherical MCM-48 mesoporous silica nanoparticles with controlled particle size. Chem Mater 22:5093–5104. https://doi.org/10.1021/cm1017344

Kleitz F, Choi SH, Ryoo R (2003) Cubic *Ia3d* large mesoporous silica: synthesis and replication to platinum nanowires, carbon nanorods and carbon nanotubes. Chem Commun:2136–2137. https://doi.org/10.1039/b306504a

Kobler J, Möller K, Bein T (2008) Colloidal suspensions of functionalized mesoporous silica nanoparticles. ACS Nano 2:791–799. https://doi.org/10.1021/nn700008s

Kuśtrowski P, Chmielarz L, Dziembaj R, Cool P, Vansant EF (2005) Modification of MCM-48-, SBA-15-, MCF-, and MSU-type mesoporous silicas with transition metal oxides using the molecular designed dispersion method. J Phys Chem B 109:11552–11558. https://doi.org/10.1021/jp050696o

Lang N, Tuel A (2004) A fast and efficient ion-exchange procedure to remove surfactant molecules from MCM-41 materials. Chem Mater 16:1961–1966. https://doi.org/10.1021/cm030633n

Lelong G, Bhattacharyya S, Kline S, Cacciaguerra T, Gonzalez MA, Saboungi M-L (2008) Effect of surfactant concentration on the morphology and texture of MCM-41 materials. J Phys Chem C 112:10674–10680. https://doi.org/10.1021/jp800898n

Lind A, du Fresne von Hohenesche C, Smått J-H, Lindén M, Unger KK (2003) Spherical silica agglomerates possessing hierarchical porosity prepared by spray drying of MCM-41 and MCM-48 nanospheres. Microporous Mesoporous Mater 66:219–227. https://doi.org/10.1016/j.micromeso.2003.09.011

Luo L, Liang Y, Erichsen ES, Anwander R (2017) Monodisperse mesoporous silica nanoparticles of distinct topology. J Colloid Interface Sci 495:84–93. https://doi.org/10.1016/j.jcis.2017.01.107

Möller K, Kobler J, Bein T (2007) Colloidal suspensions of nanometer-sized mesoporous silica. Ad. Funct Mater 17:605–612. https://doi.org/10.1002/adfm.200600578

Nandy S, Kundu D, Naskar MK (2014) Synthesis of mesoporous Stöber silica nanoparticles: the effect of secondary and tertiary alkanolamines. J Sol-Gel Sci Techn 72:49–55. https://doi.org/10.1007/s10971-014-3420-7

Nooney RI, Thirunavukkarasu D, Chen Y, Josephs R, Ostafin AE (2002) Synthesis of nanoscale mesoporous silica spheres with controlled particle size. Chem Mater 14:4721–4728. https://doi.org/10.1021/cm0204371

Pajchel L, Kolodziejski W (2018) Synthesis and characterization of MCM-48/hydroxyapatite composites for drug delivery: ibuprofen incorporation, location and release studies. Mat Sci Eng C-Mater 91:734–742. https://doi.org/10.1016/j.msec.2018.06.028

Pardo-Tarifa F, Montes V, Claure M, Cabrera S, Kusar H, Marinas A, Boutonnet M (2017) Silica with 3D mesocellular pore structure used as support for cobalt Fischer-Tropsch catalyst. Synth Catal 2:1–11. https://doi.org/10.4172/2574-0431.100017

Peng R, Zhao D, Dimitrijevic NM, Rajh T, Koodali RT (2012) Room temperature synthesis of Ti-MCM-48 and Ti-MCM-41 mesoporous materials and their performance on photocatalytic splitting of water. J Phys Chem C 116:1605–1613. https://doi.org/10.1021/jp210448v

Polshettiwar V, Cha D, Zhang X, Basset JM (2010) High-surface-area silica nanospheres (KCC-1) with a fibrous morphology. Angew Chem Int Ed 49:9652–9656. https://doi.org/10.1002/anie.201003451

Qiao Z-A, Zhang L, Guo M, Liu Y, Huo Q (2009) Synthesis of mesoporous silica nanoparticles via controlled hydrolysis and condensation of silicon alkoxide. Chem Mater 21:3823–3829. https://doi.org/10.1021/cm901335k

Schiller R, Weiss CK, Geserick J, Hüsing N, Landfester K (2009) Synthesis of mesoporous silica particles and capsules by miniemulsion technique. Chem Mater 21:5088–5098. https://doi.org/10.1021/cm901858v

Schubert U (2015) Chemistry and fundamentals of the sol–gel process. Wiley-VCH, Weinheim

Shahbazi MA, Herranz B, Santos HA (2012) Nanostructured porous Si-based nanoparticles for targeted drug delivery. Biomatter 2:296–312. https://doi.org/10.4161/biom.22347

Solovyov LA, Belousov OV, Dinnebier RE, Shmakov AN, Kirik SD (2005) X-ray diffraction structure analysis of MCM-48 mesoporous silica. J Phys Chem B 109:3233–3237. https://doi.org/10.1021/jp0482868

Stöber W, Fink A, Bohn E (1968) Controlled growth of monodispersed silica spheres in the micron size range. J Colloid Interface Sci 26:62–69. https://doi.org/10.1016/0021-9797(68)90272-5

Uhlig H, Gimpel M-L, Inayat A, Gläser R, Schwieger W, Einicke W-D, Enke D (2013) Transformation of porous glasses into MCM-41 containing geometric bodies. Microporous Mesoporous Mater 182:136–146. https://doi.org/10.1016/j.micromeso.2013.08.035

Uhlig H, Muenster T, Kloess G, Ebbinghaus SG, Einicke W-D, Gläser R, Enke D (2018) Synthesis of MCM-48 granules with bimodal pore systems via pseudomorphic transformation of porous glass. Microporous Mesoporous Mater 257:185–192. https://doi.org/10.1016/j.micromeso.2017.08.033

Urata C, Aoyama Y, Tonegawa A, Yamauchi Y, Kuroda K (2009) Dialysis process for the removal of surfactants to form colloidal mesoporous silica nanoparticles. Chem Commun:5094–5096. https://doi.org/10.1039/B908625K

Ver Meer MA, Narasimhan B, Shanks BH, Mallapragada SK (2010) Effect of mesoporosity on thermal and mechanical properties of polystyrene/silica composites. ACS Appl Mater Interfaces 2:41–47. https://doi.org/10.1021/am900540x

Verho O, Gao F, Johnston EV, Wan W, Nagendiran A, Zheng H, Bäckvall J-E, Zou X (2014) Mesoporous silica nanoparticles applied as a support for Pd and Au nanocatalysts in

cycloisomerization reactions. APL Mater 2:113316. https://doi.org/10.1063/1.4901293

Vinu A, Gokulakrishnan N, Balasubramanian VV, Alam S, Kapoor MP, Ariga K, Mori T (2008) Three-dimensional ultralarge-pore IA3d mesoporous silica with various pore diameters and their application in biomolecule immobilization. Chem Eur J 141:1529–11538. https://doi.org/10.1002/chem.200801304

Wang Y, Sun L, Jiang T, Zhang J, Zhang C, Sun C, Deng Y, Sun J, Wang S (2014) The investigation of MCM-48-type and MCM-41-type mesoporous silica as oral solid dispersion carriers for water insoluble cilostazol. Drug Dev Ind Pharm 40:819–828. https://doi.org/10.3109/03639045.2013.788013

Xu B, Ju Y, Song G, Cui Y (2013) tLyP-1-Conjugated mesoporous silica nanoparticles for tumor targeting and penetrating hydrophobic drug delivery. J Nanopart Res 15:2105–2112. https://doi.org/10.1007/s11051-013-2105-4

Yanes RE, Tamanoi F (2012) Development of mesoporous silica nanomaterials as a vehicle for anticancer drug delivery. Ther Deliv 3:389–404. https://doi.org/10.4155/tde.12.9

Zhang K, Zhang Y, Hou Q-W, Yuan E-H, Jiang JG, Albela B, He M-Y, Bonneviot L (2011) Novel synthesis and molecularly scaled surface hydrophobicity control of colloidal mesoporous silica. Microporous Mesoporous Mater 143:401–405. https://doi.org/10.1016/j.micromeso.2011.03.026

Zhang L, Zhang G, Wang S, Peng J, Cui W (2017) Sulfoethyl functionalized silica nanoparticle as an adsorbent to selectively adsorb silver ions from aqueous solutions. J Taiwan Inst Chem E 71:330–337. https://doi.org/10.1016/j.jtice.2017.01.001